Annals of Biomedical Engineering, Vol. 27, pp. 763–773, 1999
Printed in the USA. All rights reserved.
0090-6964/99/27(6)/763/11/$15.00

Vortex Shedding in Steady Flow Through a Model of an Arterial Stenosis and Its Relevance to Mural Platelet Deposition

DANNY BLUESTEIN,[1] CARLOS GUTIERREZ,[2] MATEO LONDONO,[2] AND RICHARD T. SCHOEPHOERSTER[2]

[1]Program in Biomedical Engineering, State University of New York at Stony Brook, Stony Brook, NY and [2]Mechanical Engineering Department, Florida International University, Miami, FL

(Received 22 April 1999; accepted 11 August 1999)

Abstract—In this study, the development of unsteady vortical formations in the separated flow region distal to a stenosis throat is presented and compared with the platelet deposition measurements, to enhance our understanding of the mechanisms involved in platelet kinetics in flowing blood. Qualitative and quantitative flow visualization and numerical simulations were performed in a model of a streamlined axisymmetric stenosis with an area reduction of 84% at the throat of the stenosis. Measurements were performed at Reynolds numbers (Re), based on upstream diameter and average velocity, ranging from 300 to 1800. Both the digital particle image visualization method employed and the numerical simulations were able to capture the motion of the vortices through the separated flow region. Periodic shedding of vortices began at approximately Re=375 and continued for the full range of Re studied. The locales at which these vortices are initiated, their size, and their life span, were a function of Re. The numerical simulations of turbulent flow through the stenosis model entailed a detailed depiction of the process of vortex shedding in the separated flow region downstream of the stenosis. These flow patterns were used to elucidate the mechanisms involved in blood platelet kinetics and deposition in the area in and around an arterial stenosis. The unsteady flow development in the recirculation region is hypothesized as the mechanism for observed changes in the distribution of mural platelet deposition between Re =300, 900, and 1800, despite only a marginal variation in the size and shape of the recirculation zone under these flow conditions. © *1999 Biomedical Engineering Society.* [S0090-6964(99)00306-9]

Keywords—Blood flow, Cardiovascular pathologies, Platelet activation and aggregation, CFD, DPIV.

INTRODUCTION

The coagulation of blood is a normal hemostatic process that serves to prevent blood loss in the case of a severed or ruptured blood vessel. Coagulation is also initiated when blood components are exposed to a reactive surface, such as the synthetic surface of a cardiovascular device. Thrombus formation onto a reactive surface is initiated by the activation, adhesion, and aggregation of blood platelets.[11] Platelets are blood cells ellipsoidal in shape with an average diameter of 2–4 μm. They are present in large numbers (100,000–200,000/μl) but in small volume concentration (on the order of 1%) in whole blood. In their normal state, platelets are nonadherent to one another and the blood vessel wall. However, when induced into what is called the ''active'' state, platelets change into irregular shapes with extended pseudopods, secrete chemicals into the blood stream, and are able to bind with proteins on the surface of other platelets or proteins that have been adsorbed onto a reactive surface. Platelet activation can occur through chemical stimulation (those chemicals released by activated platelets) by contact with an above threshold concentration, contact with a reactive surface, or through mechanical stimulation via fluid shearing stress. This self-propagating process continues until a loose aggregate of platelets forms on the reactive surface.

Thromboembolic complications still comprise a significant drawback in the use of synthetic biomaterials in cardiovascular devices, such as prosthetic heart valves,[1,4] vascular grafts,[6] and ventricular assist devices.[15] Flow through such devices produces contraction and curvature of streamlines and periodic vortex shedding. It has long been known that the process of thrombosis may be affected by a series of rheological and fluid dynamic parameters, including high rates of shear, areas of flow stagnation or recirculation, and turbulence.[7] Stein and Sabbah[21] have correlated turbulence with thrombus formation on artificial surfaces, and Yoganathan *et al.*[29] observed thrombus formation and tissue overgrowth on explanted Bjork–Shiley heart valves in areas of low shear and stagnation in the minor outflow region of the valve.

We have previously measured[20] platelet deposition as a function of axial position along a geometrical model of an axisymmetric arterial stenosis machined from Lexan in the range of Re=300–1800. This geometry produces

Address correspondence to Danny Bluestein; electronic mail: danny.bluestein@sunysb.edu

the type of complex, nonparallel streamline flow conditions, including separation and recirculation, high shear and turbulence, and stagnation point flow, representative of flow through cardiovascular devices. The distribution of mural platelet deposition was found to be minimum at the throat of the stenosis and included an area of increased deposition downstream of the throat. These data seem to confirm the theoretical predictions of Wurzinger and Schmid-Schoenbein,[27] who used a stenosis as a model for discussion of the relevant fluid dynamic factors affecting the development of mural thrombus. In this model, local increases in shear in the throat region causes activation of platelets. Immediately downstream of the stenosis, flow separating off the throat creates a region of slowly recirculating flow conducive to aggregation of platelets and platelet-activating factors. Further downstream, the main flow reattaches to the tube wall, creating a point of primary adhesion and subsequent aggregation of the activated platelets.

In previous studies,[3] platelet deposition was correlated with flow dynamics using a steady flow numerical model to predict flow patterns. This model was unable to capture the unsteady vortex phenomena in the recirculation region known to occur under these conditions. The purpose of the current study is to fully characterize the flow within the recirculation region downstream of a tubular constriction, and to use the observed flow dynamics to elucidate the mechanisms involved in blood platelet kinetics and deposition in this region.

METHODS

Platelet Deposition

Previously measured platelet deposition results were obtained by radioactive labeling of canine blood platelets with In-111, and quantified by measuring the percentage of radioactivity bound to platelets along successive segments of a model stenosis manufactured from transparent Lexan that was installed in a recirculating flow loop. The stenosis model employed was scaled down 1/10 from the dimensions of the flow visualization model shown in Fig. 1. This smaller model size was dictated by the amount of blood volume available. By keeping dynamic similarity between the two models (the same Reynolds number) similar flow conditions were observed. A steady flow peristaltic pump recirculated the blood through the flow loop, and a water bath maintained the blood temperature at 37 °C. The platelets were labeled with In-111 tropolone using procedures described in detail by Dewanjee *et al.*[5] The results are presented in terms of normalized platelet density (NPD), where the local number of platelets per unit area is normalized by the average platelet density along the entire test chamber. Details of these methods and the results can be found in Ref. 20.

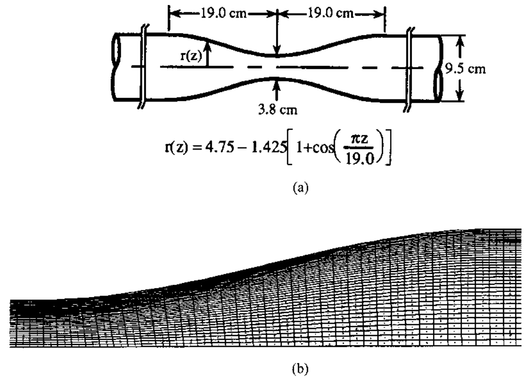

FIGURE 1. (a) The arterial stenosis model. (b) Detail of the computational mesh in the stenosis throat area. The progressive density of the mesh in the radial direction shows the carefully modeled near wall region.

Flow Visualization

Both qualitative and quantitative flow visualization measurements were performed. In order to enhance resolution, measurements were carried out in a steady flow loop with the large scale stenosis model (10 times the model size used for the blood flow measurements) shown in Fig. 1. The model, blown from glass, is a streamlined axisymmetric stenosis with an upstream tube diameter of 9.5 cm, an area reduction of 84% at the throat of the stenosis, and a stenosis length of four diameters. The steady flow loop included an entry length of 25 diameters and distal length of 16 diameters. The working fluid was water, seeded with reflective polycrystalline beads of 25 μm average diameter (Optimage Ltd., Edinburgh, UK) to visualize the flow. The density of the beads was identical to that of the working fluid. The seeding particles were 25 μm, which is around 10 times the average size of a platelet. Geometric and dynamic similarity was maintained between the platelet deposition measurements and the flow visualization. The field was illuminated with a 500 mW argon-ion laser and a cylindrical lens that produces a 1.5-mm-thick light sheet. The plane of view was a slice through the center of the axisymmetric flow chamber. Qualitative flow visualization was recorded on videotape for a range of flow rates corresponding to Reynolds numbers (Re, based on upstream diameter and average velocity) of Re=300–1800. The range of Re considered is relevant to both certain pathological conditions in the cardiovascular system, e.g., carotid stenosis combined with hypertension and/or anemia, and flow through cardiovascular devices such as ventricular assist devices and prosthetic heart valves.

Velocity vector field measurements described in this paper were taken using the Flowgrabber digital particle image velocimetry (DPIV) system (Dantec Measurement Technology Inc., Mahwah, New Jersey). The system consists of a 500 mW argon-ion laser: a cylindrical lens which produces a 1.5-mm-thick sheet; a mechanical shutter, fixed 30 Hz frame rate charge-coupled device (CCD) camera with frame size 512 by 480 pixels, and a timing box interface to reduce exposure time and time between frames to a minimum of 2 ms; a PC with frame-grabbing board; and the Flowgrabber software for computation and presentation of the velocity vector fields. The method used to compute velocities is described in detail by Willert and Gharib.[26]

The method may be summarized as follows. Two sequential digitally recorded video images of seed particles within the light sheet in the flow, using an exposure time and frame rate such that the particles are visualized without a streakline and with optimal motion of the particles (around 5–10 pixels maximum), are single exposed. The two images are subsampled at one particular area via an interrogation window (usually 32×32 pixels). Within these image samples an average spatial shift of particles may be observed from one sample to its counterpart in the other image. This shift may be obtained by performing a spatial cross-correlation of the two images. The maximum cross-correlation peak coincides with the location of the displacement delta function. A broad correlation peak allows subpixel accuracy using a centroiding technique. The sampling window is overlapped 50% with the next, resulting in a grid of approximately 960 equally spaced (16 pixels) displacement vectors for each image pair.

Numerical Methods

Computational fluid dynamics (CFD) modeling of transient turbulent flow was employed. The blood was modeled as a viscoelastic fluid, with yield a stress of 0.1 s^{-1} and a changing viscosity with physiological blood properties. The changing blood viscosity as a function of shear rate (approximating $\rho = 1.056\ \mathrm{g/cm^3}$, $\mu = 3.5$ cPoise, and $\nu = 0.035\ \mathrm{cm^2/s}$ at elevated shear levels) was curve fitted to data measured in humans by Merrill *et al.*(1966)[14] and incorporated into the numerical model. This is a crucial point for capturing accurately the dynamics of shed vortices, which are characterized by a low shear stress environment. A quasi-unsteady flow condition was employed at the inlet, by applying a 5% fluctuation over a period of 10 ms to the inlet velocity profile. This boundary condition was intended for inducing an instability at the shear layer formed between the stenotic jet flow and the recirculation zone, that would initiate vortex shedding. A range of fluctuation levels and periods was tested, e.g., 0.15% fluctuation over periods of 10 and 2.5 ms, and was found to produce very similar results. This conforms with Hussain,[12,13] who studied vortex shedding in the presence of controlled excitation and concluded that pulsation over a wide range of frequencies had no effect on the natural shedding frequency.

The numerical simulations were conducted using the FIDAP CFD package (Fluent Inc., Lebanon, NH) that utilizes a finite element procedure, using the Galerkin form of the method of weighted residuals[19] to solve the Navier–Stokes (N.S.) and continuity equations:

$$\rho\left(\frac{\partial u_i}{\partial t} + u_j u_{i,j}\right) = \sigma_{ij,i} + \rho f_i \tag{1}$$

$$\frac{\partial \rho}{\partial t} + (\rho u_j)_j = 0. \tag{2}$$

In turbulent flows all variables in the governing N.S. equations are decomposed into average values and small fluctuations, e.g., $u = \overline{U} + u'$, where the overbar denotes time average and the prime denotes fluctuation from this average. When these variables are substituted into Eq. (1) and time averaging is performed, a resulting extra variable is introduced to the stress terms, i.e., the Reynolds stresses $\rho\overline{u'v'}$. To close the number of governing equations with the extra variables, the two-equation k-ϵ turbulence model is traditionally employed. In the k-ϵ turbulence model the turbulent field is characterized in terms of the turbulent kinetic energy k, and the viscous dissipation rate of turbulent kinetic energy ϵ, which are defined as

$$k = \tfrac{1}{2}\,\overline{u_i u_i}, \tag{3}$$

$$\epsilon = \nu\,\overline{u_{i,j} u_{i,j}}. \tag{4}$$

Two transport equations, one for k and one for ϵ, are obtained from the N.S. equations and the new system of equations is then solved. While this approach is very efficient and accurate for high-Re flows, it may produce inferior predictions for some low-Re flows. As physiological flows are exclusively in the low Re range, the innovative Wilcox k-ω model,[24,25] which is primarily intended for simulating globally low-Re internal flows (Re<10,000) was employed. In this model the turbulent dissipation is related to the turbulent kinetic energy via the simple expression $\epsilon = \omega k$, where ω is the turbulent frequency. The turbulent scales u_t and δ_t are related through dimensional analysis to k and ω according to $u_t \propto \sqrt{k}$ and $\delta_t \propto \sqrt{k}/\omega$. The turbulent viscosity is obtained from the k-ω relation; $\mu_t = \mu\rho k/\omega$, and the k-ω transport equations are solved.

A progressive mesh density in the axial direction was applied to the inlet region, so that flow conditions at the inlet could be altered from a uniform flow velocity profile to a fully developed turbulent velocity profile where turbulence prevailed. A zero stress zero pressure condition was applied at the outlet, and a no-slip condition

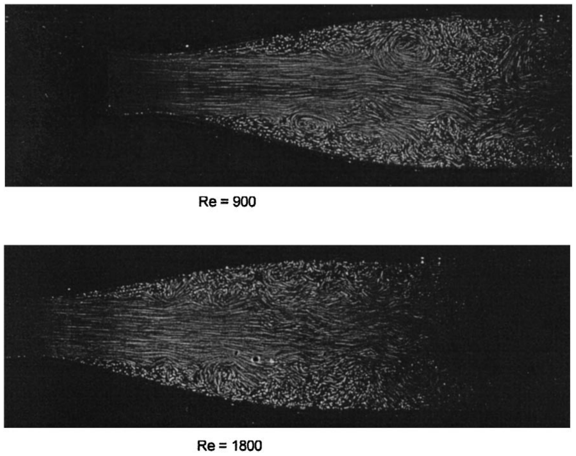

FIGURE 2. Photographs of vortex shedding distal the stenosis throat. For Re=900 the vortices meander in the interface between the core jet and the slowly recirculating fluid. For Re=1800 the point of inception of the shed vortices is further upstream, and the vortices meander closer to the stenosis wall.

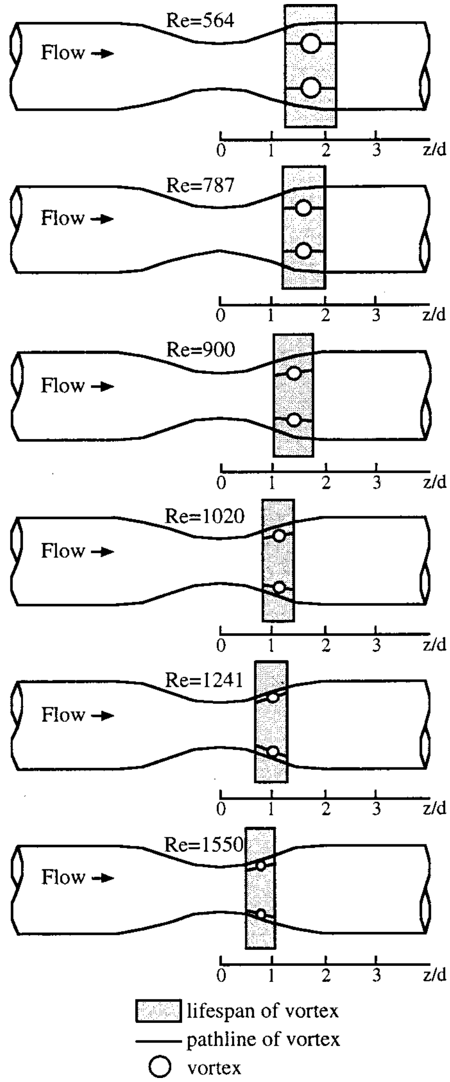

FIGURE 3. Schematic drawing of the relative location, pathline, and size of the vortices observed at representative Re beginning at the inception of observable and repeatable periodic vortex formation. At Re>1600, the vortex formation was not visually observable because of the increasing disturbance of the flow in the recirculation region.

was applied at the walls. The entrance length was conservatively chosen as 5 diameters so that the velocity profiles could be fully established proximal to the stenosis. To find the exit tube length, we examined wall stresses on the stenosis and the axial velocity profile in the center of the model. Results were independent of exit length for total model length greater than 10 diameters. We conservatively selected a model length of 16.8 diameters (5 diameters entry length, 3.8 diameters stenosis section, and 8 diameters exit length). The progressive density and resolution of the finite elements mesh in the radial direction was dictated by the need in the k-ω model of the first grid point away from the walls to be in the vicinity of $y^+ \leqslant 1$ (y^+ being the nondimensional viscous sublayer height). The height of Δ, the first grid point from the wall, was computed in the following manner:[24,25]

$$\omega = \frac{6\nu}{C_2 \Delta^2}, \tag{5}$$

where C_2 is an empirical constant. With a computed characteristic near wall turbulent dissipation rate of $\epsilon = 50{,}613\ \mathrm{mm}^2/\mathrm{s}^3$ and $C_2 = 0.8333$, the $\epsilon = \omega k$ relation with a typical turbulent kinetic energy of $k = 4050\ \mathrm{mm}^2/\mathrm{s}^2$ yielded a characteristic turbulent frequency of $\omega = 125\ \mathrm{s}^{-1}$. These values put Δ at a characteristic value of 140 μm which was used to determine the minimal mesh density in the vicinity of the wall.

After establishing the numerical results to be independent of mesh density in all directions, the two-dimensional (2D) mesh, solved in half of the flow domain, consisted of some 4500 quadrilateral elements each containing nine nodes, i.e., 40,500 computational nodes. The resulting mesh is shown in Fig. 1, in the vicinity of the stenosis. The choice of a transient analysis time integration algorithm is governed by its rate of convergence and sensitivity to variations in the initial conditions. The choice of the segregated version of the solver, combined with a hybrid relaxation method and streamline upwinding was successful in achieving convergence for the demanding combination of a transient problem and turbulence modeling. The time step was set constant at 0.1×10^{-3} s.

Turbulent particle paths were computed using a stochastic model[9] that simulates the influence of turbulence on particle trajectories. In this model the instantaneous

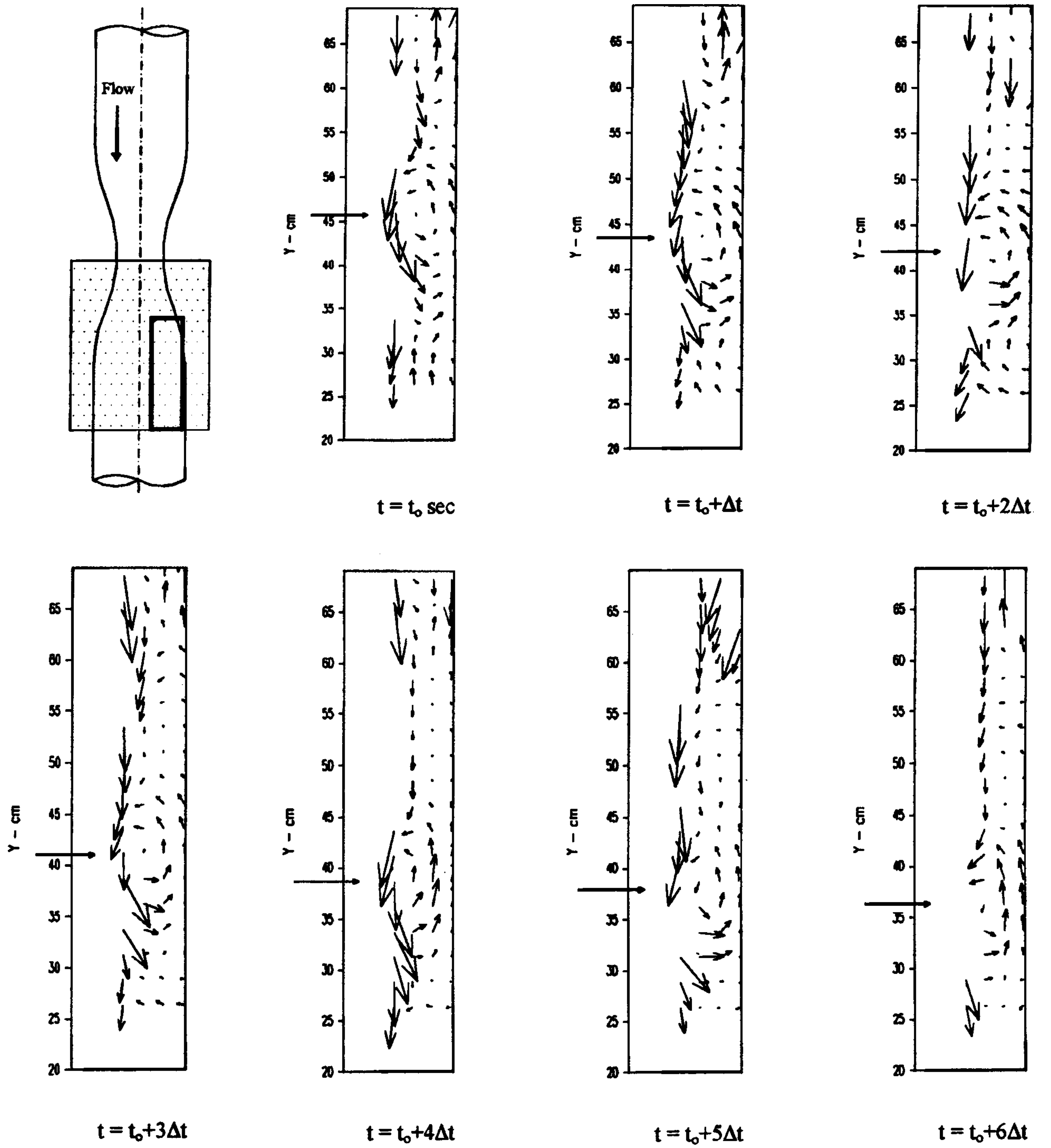

FIGURE 4. Motion of a typical periodic vortex as it travels along the core jet (in the *y* direction) at Re=564. The first frame is a schematic of the test chamber showing the region of visualized flow (shaded region), and the particular region of interest in which DPIV calculations were performed (rectangular box—the interrogation area is 4 cm wide). Flow is from top to bottom in each frame, and the higher jet velocities have been clipped. The arrow on the vertical axis marks the approximate location of the vortex center. The Δt between each frame was 267 ms.

velocities in the carrier phase are used to solve the particle velocities. These instantaneous characteristics are computed by adding random fluctuations obtained from the k-ω simulation, in the following manner:

$$U_\infty = \overline{U} + \lambda u'; \quad u' = \sqrt{(\tfrac{2}{3}k)}, \tag{6}$$

where λ is a random number between -1 and 1 sampled

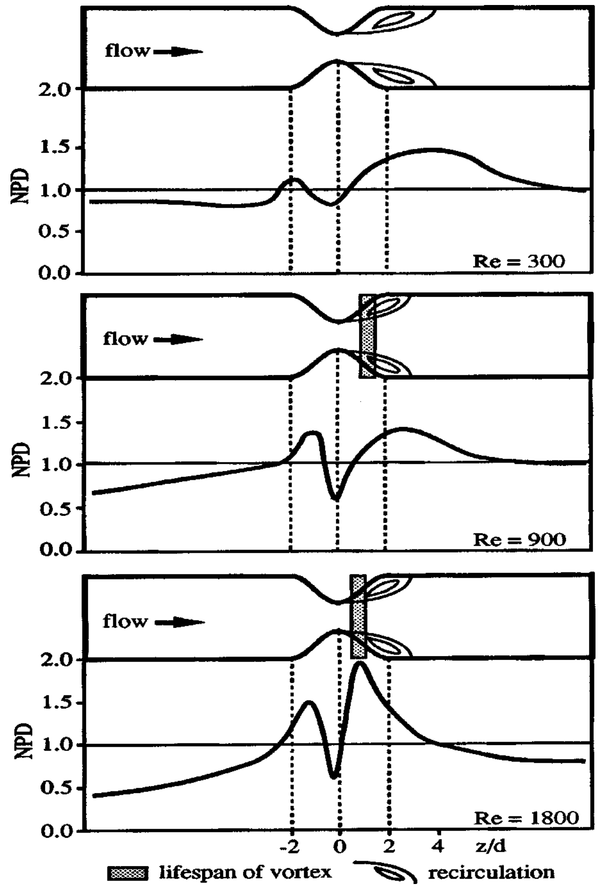

FIGURE 5. Normalized platelet density (NPD), at the three different Re at which NPD measurements were made, compared with flow conditions in the recirculation region. At Re=300, no vortex shedding occurred, and the distal region of increased NPD is centered around the reattachment point. At Re=900, vortex shedding occurred, but the vortices did not affect near wall dynamics, and thus the distal region of increased NPD is again centered around the point of reattachment. Finally, at Re=1800, vortex shedding occurred near the separation region at the stenosis model wall, obviously affecting near wall platelet kinetics and resulting in a very localized increase in NPD in this region.

from a normal distribution. The motion of each particle is traced as it interacts with a succession of turbulent eddies. The interaction time with one eddy is limited to the eddy lifetime-Te, or the time needed for the particle to traverse the eddy-T_t, defined by

$$\mathrm{Te}=\frac{\mathrm{Le}}{\sqrt{\frac{2}{3}k}};\quad T_t=-2\ln\left(1-\frac{\mathrm{Le}}{\tau|U_\infty-U_p|}\right),\qquad(7)$$

where $\mathrm{Le}=(c^{3/4}k^{3/2})/\epsilon$ is the eddy characteristic size and τ is the particle relaxation time. After each interaction, a new fluctuation is assumed to act on the particle, i.e., the particle enters a new eddy. Unlike laminar flow numerical simulations which yield exactly the same particle

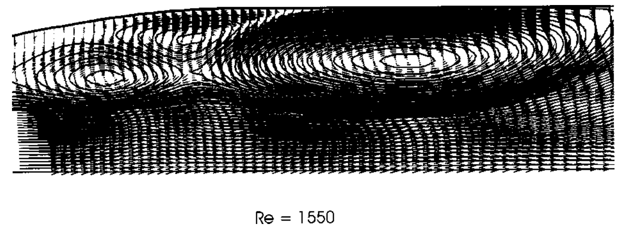

FIGURE 6. Velocity vectors with streamlines superimposed on them at Re=1550 depict an intricate pattern of shed vortices that roll on top of each other and merge in the expansion zone distal to the stenosis throat.

path when a particle is repeatedly injected at a certain point in the flow field, the combination of turbulence modeling and a stochastic model for turbulent particle paths computations result in a different particle path for each run, as should be the case under turbulent flow conditions.

RESULTS

Flow Visualization

The phenomenon of periodic shedding of vortices in the separated region downstream of the stenosis throat began at approximately Re=375 and continued for the full range of Re studied. Characteristic patterns of the shed vortices are shown in photographs of the flow visualization for Re=900 and 1800 (Fig. 2). For Re=900 the vortices meander in the interface between the core jet and the slowly recirculating fluid. For Re=1800 the point of inception of the shed vortices is further upstream, and the vortices meander closer to the stenosis wall. In general, the location of the site at which these vortices are initiated, the size of the vortex, and the life of the vortex varies with Re (Fig. 3). At low Re (564), the vortex ring is not formed at the point of separation but further downstream of the throat within the shear layer between the jet and recirculating region of flow, and the vortex meanders, in a direction roughly parallel to the cylindrical axis, through the separated flow region until merging with the main flow near the reattachment point approximately three diameters downstream. For Re <1000, the vortex ring remains confined between the core jet and a layer of slowly moving fluid near the wall. As Re increases, the location of the roll formation moves upstream and closer to the wall, such that, for Re>1000, the site of vortex initiation is very near the stenosis throat at the point of flow separation. At this range of Re, the vortex is much smaller, rotates at a much faster rate, and dissipates before reaching the end of the stenosis region. The path of the vortex ring at Re>1000 is pushed outward from the jet, such that it appears the vortices are rolling along the stenosis walls.

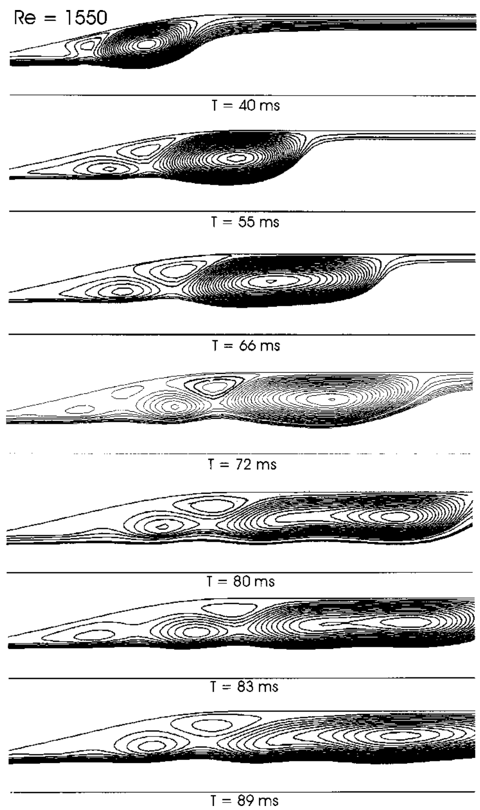

FIGURE 7. The dynamics of vortex shedding distal to the stenosis throat at Re=1550 over time. A large vortex is fully formed at $T=40$ ms, accompanied by a smaller, counter-rotating, vortex. These two vortices are convected downstream, with the second vortex rolling on top of the first ($T=55$ ms). A third newly formed vortex is trailing both vortices. The three vortices are convected together downstream ($T=66$ ms), with the third vortex starting to merge with the first. Two newly formed vortices ($T=72$ ms) trail the original three vortices structure, making it into five discernible vortices. The process of shed vortices rolling on top of each other ($T=80$ ms) and the merging of discrete vortices ($T=83$ and 89 ms), continues perpetually.

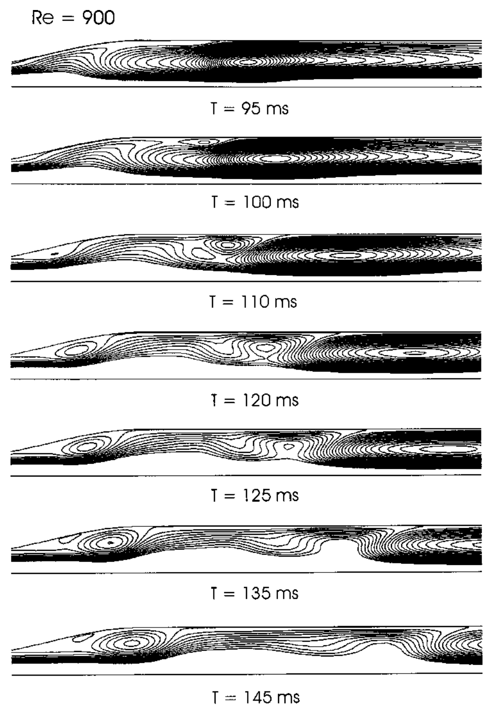

FIGURE 8. Periodic vortex shedding at Re=900 (perturbation is superimposed on an already established recirculation vortex). The recirculation vortex becomes unstable, with newly formed shed vortices trailing it ($T=100$ and 110 ms), while newly formed vortices at the expansion zone of the stenosis ($T=110$–145 ms) are convected downstream.

DPIV measurements of the motion of a typical periodic vortex as it travels along the core jet at Re=564 is shown in Fig. 4. At this Re, the vortex is shown to move a distance of approximately 9.5 cm, or about 1 diameter, in the span of 1.6 s. This corresponds to an average speed of 5.94 cm/s for the center of the vortex. The DPIV measurements capture the rotational aspects of the vortex in a satisfactory manner. Note the increased retrograde velocities in the vortex compared with the velocities of particles located within the region of recirculation but not rotating with the vortex. However, these velocities are still much slower than velocities of the particles rotating with the vortex but located within the core jet. As shown in Fig. 2, at the lower Reynolds numbers the vortices remain confined between the core jet and a layer of slowly moving fluid near the wall. Therefore, one may model the motion of the vortex as a rigid cylinder rolling without slip between two moving plates moving in opposite directions and at different speeds. The velocity vector field at the location of the vortex resembles the velocities of individual points on the surface of the cylinder model, with deviations occurring due to fluid deformation, particularly along the edge of the jet.

Numerical Simulations

Results are shown for Re=1550 and 900 (Figs. 6–10). Velocity vectors with streamlines superimposed on them (Fig. 6, Re=1550) reveal an intricate pattern of shed vortices that roll on top of each other and merge in the expansion zone distal to the stenosis throat. While a large steady vortex encompassing the complete recirculation region (from the flow separation point to the reattachment point) was reported by numerous researchers over the years, this depiction indicates that the flow dynamics in the recirculation region are more complex. The large vortex on the right, reminiscent of the steady recirculation vortex, is accompanied by two smaller counter-rotating vortices in a form characteristic of periodic vortex shedding (von-Kármán vortex street) in wakes of bluff bodies and shear flows.[23]

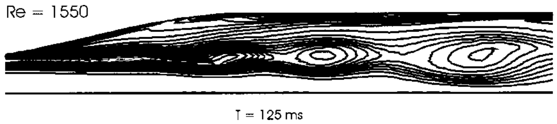

FIGURE 9. Vorticity contours at Re=1550. The vortical activity is depicted by the closed isovorticity contours. The centers of isovorticity are located at the shear layer between the vortices and the stenotic jet.

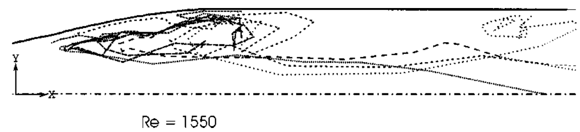

FIGURE 10. Turbulent particle paths simulations at Re=1550 (from T=40 to 89 ms). The bulk of the particles that were seeded in the expansion region were entrapped within the smaller, counter-rotating, shed vortices, while a small part of the particles wandered to the bigger recirculation vortex downstream. Once entrapped in these vortices, most of these particles were eventually convected toward the wall; only two out of eight computed trajectories lead the particles away from the wall.

The dynamics of vortex shedding distal to the stenosis throat at Re=1550 are depicted in Fig. 7 over time. A large vortex is fully formed at $T=40$ ms, accompanied by a smaller, counter-rotating, vortex. These two vortices are convected downstream, with the second vortex rolling on top of the first ($T=55$ ms). A third newly formed vortex is trailing both vortices. The three vortices are convected together downstream ($T=66$ ms), with the third vortex starting to merge with the first. Two newly formed vortices ($T=72$ ms) are now trailing the original three vortices structure, making it into five discernible vortices. This process of shed vortices rolling on top of each other ($T=80$ ms) and the merging of discrete vortices ($T=83$ and 89 ms), continues perpetually. A similar depiction of periodic vortex shedding is shown in Fig. 8 for Re=900, where the 5% velocity fluctuation at the inlet was imposed on an already established steady recirculation vortex. As a result the recirculation vortex becomes unstable, with newly formed shed vortices trailing it ($T=100$ and 110 ms), while newly formed vortices at the expansion zone of the stenosis ($T=110$–145 ms) are convected downstream.

In addition to the streamlines and the velocity vector field, the level of the vorticity in the flow field is an important measure of the vortical flow components. Vorticity is defined as $\vec{\omega}=\nabla\times\vec{U}$, where for a 2D flow field, the vorticity is computed as $\omega=\partial v/\partial x-\partial u/\partial y$. The vorticity field is outlined in Fig. 9, where the vortical activity is depicted by the closed isovorticity contours. The centers of isovorticity are located at the shear layer between the vortices and the stenotic jet. The maximum local vorticity at the core of the vortices reached values as high as 350 s^{-1}, indicating the strong vortical activity that was induced by the shed vortices. Generally, the vorticity alternated between positive and negative values, typical of the ''von-Kármán vortex street'' dynamics in which successive vortices rotate at alternating clockwise and counterclockwise motion.

To study the effect of these flow dynamics on platelet trajectories within the recirculation region, turbulent particle paths simulations were conducted. Several such particle paths are shown in Fig. 10 for Re=1550 (from T=40 to 89 ms). The bulk of the particles that were seeded in the expansion region near the wall were entrapped within the smaller, counter-rotating, shed vortices, while a small part of the particles wandered to the bigger vortex downstream. Once entrapped in these vortices, most of these particles were eventually convected toward the wall.

Platelet Deposition

The unsteady flow development in the recirculation region may be the mechanism for significant changes in the distribution of mural platelet deposition between Re =300, 900, and 1800, despite only a marginal variation in the size and shape of the recirculation zone under these flow conditions (Fig. 5). At Re=300, a recirculation zone was formed which extended approximately 3.5 diameters downstream from the throat and consisted of slowly recirculating flow enclosed in a single, elongated vortex ring. Platelet deposition (NPD) displayed a slight increase proximal to the stenosis throat, a slight decrease at the throat, and a large increase distal to the throat. The distal region of increased NPD corresponded approximately to the length of the recirculation region. At Re =900, the reattachment point moved to approximately three diameters downstream of the throat, and varied little more with further increases in Re. However, for Re=900 and 1800, vortex shedding occurred. The pathline of the vortex at Re=900 is shown in Fig. 3, while for Re=1800 the path of the vortex was similar to the path shown for Re=1550 in Fig. 3. The pattern for platelet deposition continued for the two higher Re, with a proximal increase, decrease at the throat, and distal increase. For Re=900, the distal region of increased NPD corresponded with the length of the recirculation zone, as the results for Re=300 displayed. However, at Re=1800, the region of increased NPD was much nearer to the throat, higher in magnitude, and corresponded with the region of vortex formation.

DISCUSSION

The development of unsteady flow structures in separation has been observed in a variety of applications. The classical example is the Karman vortex sheet known to occur in flow past a circular cylinder in the $10^3<\mathrm{Re}<10^7$ range.[23] Pauley *et al.*[18] solved the unsteady Navier–Stokes equations for flow through a channel in which suction was applied on one wall, exposing the opposite wall to an adverse pressure gradient resulting in separation of the flow from the wall surface. For relatively weak adverse pressure gradients, the observed separated region was described as a thin, steady, closed separation bubble. Stronger adverse pressure gradients (caused by increased suction) led to vortex shedding. Fearn *et al.*[8] observed vortex shedding downstream of a symmetric sudden expansion under steady flow conditions. The flow remained steady and symmetric for $\mathrm{Re}<35$, then became asymmetric for $\mathrm{Re}<155$, at which point vortex shedding ensued. Experimental observations indicated that the time dependence was a result of a three-dimensional disturbance. Fearn *et al.*[8] also studied numerically the effect of inducing a 1% velocity perturbation, representing the small imperfections inevitable in their experimental apparatus, on the flow stability and the development of vortices and recirculation zones distal to the expansion. They found that the perturbation had a considerable effect on all of the above. At higher Re numbers vortex shedding ensued, with the position of the shedding moving upstream along the shear layer between the recirculation zone and the core flow.

The transition to unsteadiness has also been observed in flows through biomechanical structures. Ojha[16] noted the transition of the separation structure, within a 45° anastomotic junction, from a single bubble at $\mathrm{Re}=250$, to a corotating dual-vortex structure at $\mathrm{Re}=500$, to finally the onset of unsteadiness that included vortex shedding for $\mathrm{Re}>1000$. Vortex shedding has also been shown to occur off the trailing edge of the leaflets of a bileaflet heart valve prostheses in the deceleration flow phase of the heart cycle.[10] Finally, flow through an arterial stenosis has been studied in great detail by Young.[30] The most detailed steady flow measurements at Re corresponding with the current study were performed by Ahmed and Giddens.[2] For flow through a 75% stenosis, flow was stable and laminar at $\mathrm{Re}=250$, experienced periodic oscillations at $\mathrm{Re}=500$, and poststenotic turbulence at $\mathrm{Re}=1000$ and higher. These results as well as those discussed above with similar conditions of separation agree with the results of the current study. A stable, single vortex structure was observed at $\mathrm{Re}=300$, with vortex shedding ensuing with increasing Re. Conducting numerical simulations in a stenosis geometry, Thornburg *et al.*[22] observed vortex shedding distal to the stenosis throat under steady flow conditions. No study that we are aware of has captured the details of the shedding vortices as displayed here with the DPIV measurements, or demonstrated their existence in a stenosis geometry using a numerical perturbed *turbulent* flow simulation.

In previous work by Schoephoerster *et al.*[20] and Bluestein *et al.*[3] platelet deposition was correlated with local fluid dynamics obtained by numerical solution of the equations governing flow through a stenosis. The numerical solution was obtained assuming steady flow, and thus produced a single, closed vortex within the recirculation region. The size of the recirculation region and the velocities in the main flow were validated with DPIV measurements. The postulated flow-induced mechanisms for platelet deposition in a stenosis geometry included: (1) enhanced convective transport of platelets to the wall along locally curved streamlines with velocity components perpendicular to the wall; (2) platelet activation by above-threshold values of shear stress; and (3) local wall shear stresses, which, if high, may wash adhered platelets from the wall or, if low, may allow prolonged contact of platelets with the wall. These mechanisms were used to explain the observed distribution of platelet deposition obtained (Fig. 5). Enhanced convective transport occurred both proximal and distal to the stenosis throat and was considered causative to the increases in deposition at those locations. The decreases in platelet deposition at the throat was thought to be attributable to the local high wall shear stress which is likely to wash the platelets from the surface. Finally, the size of the distal region of increased platelet deposition correlated very well with the size of the recirculation zones, at least for $\mathrm{Re}=300$ and 900. This was thought to be due to a diminished capacity for the flow to wash the platelets away from the surface because of low wall shear in the recirculation region, as well as prolonged contact of platelets with the surface in the layer of slow moving fluid near the wall.

However, the size of the recirculation region remained essentially the same for $\mathrm{Re}=900$ and 1800. Despite that, the size and magnitude of the distal region of increased platelet deposition changed remarkably between these two flow conditions. We now postulate that this change in platelet deposition pattern may be attributable to the vortex shedding phenomena. The shedding of vortices in the shear layer between the core jet and the recirculation region began above $\mathrm{Re}=375$ and continued through $\mathrm{Re}=1800$. In addition, the location of vortex initiation as well as the path of the vortices varied with Re. With this in mind, the following mechanisms involving the vortex shedding may be postulated. At $\mathrm{Re}=300$, no vortex shedding occurred, and thus the previously mentioned mechanisms are sufficient to explain the observed platelet deposition. At $\mathrm{Re}=900$, vortex shedding did occur. However, as noted previously, the path of the vortices at this Re was clearly separated from the wall as shown in Fig. 3. In this case, the vortex moved between the core jet and a slowly moving layer of fluid near the stenosis wall. Therefore, the vortex did not affect near wall dynamics, and the mechanisms previously mentioned still hold. For Re=1800, the vortex path resembled that of Re=1550 in Fig. 3. Here the vortex appeared to roll directly along the stenosis wall. In the area of the wall near this rolling vortex, convective transfer of fluid and platelets towards the wall will be enhanced. As shown in Fig. 5, the location within the stenosis of the lifespan of the vortices for Re=1800 coincides with the relatively narrow region of increased platelet deposition just distal to the stenosis throat. This is further supported by the numerical simulations, which depict turbulent particle paths which lead the platelets to deposition in this region (Fig. 10). We propose that the increase of platelet deposition in this area is a result of the development of these vortical structures in the flow field near the wall at this Re range.

Therefore, the mechanisms which lead to the vortex shedding phenomenon in flow through a stenosis proceed as follows: (1) an instability mechanism characteristic of confined jets arises when the jet attempts to attach to the downstream walls.[28] The emerging jet forms a vortex sheet at the interface between the jet and the surrounding fluid. This is accompanied by an entrainment process where, in the case of the bounded jet, the fluid must come from the downstream region. As the jet expands towards this region, it attaches and breaks from the walls, causing the surrounding fluid to oscillate back and forth. These fluctuations, in turn, influence the character of the vortex sheet. (2) As at higher Re numbers the stenotic jet becomes turbulent, in the process some non-turbulent fluid is entrained, to which vorticity fluctuations are transferred by viscous diffusion.[12] Those, in turn, induce flow instabilities to the shear layer that may break the recirculation zone into discrete vortices. Flow fluctuations that may exist in the flow field will tend to be augmented in the shear layer because of the inherent instabilities. (3) Once the recirculation zone breaks down into discrete vortices, any slight nonuniformity in strengths or spacing of two (or three) adjacent vortices induces them to roll up around each other (vortex pairing).[12,13]

The numerical simulations of turbulent flow with a small fluctuation superimposed at the inlet, and the DPIV measurements, indicate that this is the case. As a result of the inherent instability at the shear layer the fluctuations are augmented, breaking down the recirculation region into discrete vortices and inducing vortex shedding. These flow conditions bear direct relevance to the flow conditions in stenosed blood vessels, where a certain degree of pulsatility is always present in the flow field.

In order to substantiate the hypothesized mechanisms for the actual platelet deposition unto the wall, we are currently developing a mathematical model of platelet kinetics and deposition in which the platelets will be modeled as particles (solid phase) in a carrier fluid. In this model platelet deposition onto surface boundaries will depend on (1) the activation state of the platelet, (2) the reactivity of the surface, and (3) the local fluid dynamic forces at the surface. It is hoped that this model can be used to verify the mechanisms postulated using the results of the previous and current studies.

The extrapolation of the observed correlations between regional dynamics of the flow and localized platelet deposition to the physiological environment must be tempered with the limitations of the *in vitro* experimental conditions in replicating *in vivo* conditions. In particular, arterial blood flow is quite pulsatile in nature. However, even under pulsatile flow conditions, vortical structures similar to those observed in these experiments have been shown to occur in the deceleration phase downstream of a tube constriction.[17] The interaction of flow with blood coagulation elements and events is extremely complex, and even steady flow through a stenosis geometry can be quite involved as we have shown. Therefore, it was our intent to develop initial correlations under steady flow conditions and a better understanding of the interaction between flow and the coagulation process before the addition of convoluted pulsatile flow effects.

CONCLUSIONS

We have shown that platelet deposition onto a model arterial stenosis can be correlated with and depends on local fluid dynamic phenomena, and that these phenomena include convection towards the wall, shearing forces within the fluid, and fluid near-wall drag. In particular, the current study depicts a process where vortex shedding occurs in the geometry studied at Re>350, that these vortices affect near wall flow only for Re>1000, and that for this higher range of Re the shed vortices enhance local platelet deposition.

ACKNOWLEDGMENTS

The work described in this paper was supported in part by grants from the National Institutes of Health (HL46444) and the American Heart Association, Florida Affiliate (9501342) (R.T.S.), and by grant No. 97-00446 from the United States-Israel Binational Science Foundation (BSF) (D.B.).

REFERENCES

[1] Addonizio, V. P., and Z. H. Edmunds. Thromboembolic complications of prosthetic valves. *Cardiovasc. Clinics.* 3:431–435, 1985.

[2] Ahmed, S. A. and D. P. Giddens. Velocity measurements in steady flow through axisymmetric stenoses at moderate Reynolds numbers. *J. Biomech.* 16:505–516, 1983.

[3] Bluestein, D., L. Niu, R. T. Schoephoerster, and M. K. Dewanjee. Fluid mechanics of arterial stenosis: Relationship to

the development of mural thrombus. *Ann. Biomed. Eng.* 25:344–356, 1997.

[4] Chandran, K. B. Heart valve prostheses: In vitro flow dynamics, in Encyclopedia for Medical Instrumentation, edited by J. G. Webster. New York: Wiley, 1988, Vol. 3, pp. 1475–1483.

[5] Dewanjee, M. K., S. A. Rao, and P. Didisheim. Indium-111 tropolone, a new platelet label: Preparation and evaluation of labeling parameters. *J. Nucl. Med.* 22:981–987, 1981.

[6] Dewanjee, M. K. In-111 platelets in bypass grafts: Experimental and clinical applications, in Radiolabeled Cellular Elements of Blood, edited by M. L. Thakur, M. Hardeman, and M. D. Ezekowitz. New York: Plenum, 1985, pp. 229–263.

[7] Dintenfass, L. Rheological approach to thrombosis and atherosclerosis. *Angiology* 15:333–343, 1964.

[8] Fearn, R. M., T. Mullin, and K. A. Cliffe. Nonlinear flow phenomena in a symmetric sudden expansion. *J. Fluid Mech.* 211:595–608, 1990.

[9] Gosman, A. D., and L. Ioannides. Aspects of computer simulation of liquid-fueled cumbustors, AIAA 19th Aerospace Science Meeting, Paper no. 81-0323, 1981.

[10] Gross, J. M., C. D. Shermer, and N. H. C. Hwang. Vortex shedding in bileaflet heart valve prostheses. *Trans. Am. Soc. Artif. Intern. Organs* 34:845–850, 1988.

[11] Guyton, A. C. Textbook of Medical Physiology, eighth ed. Philadelphia: Saunders, 1991, pp. 390–399.

[12] Hussain, A. K. M. F. Mechanics of pulsatile flows of relevance to the cardiovascular system. In Cardiovascular Flow Dynamics and Measurements, edited by N. H. C. Hwang and N. A. Norman: University Park Press, 1975, Chap. 15, pp. 541–633.

[13] A. K. M. F. Hussain. Coherent structures and turbulence. *J. Fluid Mech.* 173:303–356, 1986.

[14] Merrill, E. W., E. R. Gilliland, G. R. Cokelet, H. Shin, A. Britten, and R. E. Wells. Rheology of human blood, near and at zero flow. *Biophys. J.* 3:199–213, 1963.

[15] Muneretto, C., E. Solis, A. Pavie, P. Leger, I. Gandjbakhch, J. Szefner, V. Bors, C. Piazza, A. Cabrol, and C. Cabrol. Total artificial heart: Survival and complications, *Ann. Thorac. Surg.* 47:151–157, 1989.

[16] Ojha, M. Flow separation and the transition to unsteadiness, Advances in Bioengineering, New York: ASME, 1995, Vol. 29, pp. 347–348.

[17] Ojha, M., R. S. C. Cobbold, K. W. Johnston, and R. L. Hummel. Pulsatile flow through constricted tubes: an experimental investigation using photochromic tracer methods. *J. Fluid Mech.* 203:173–197, 1989.

[18] Pauley, L. L., P. Moin, and W. C. Reynolds. The structure of two-dimensional separation. *J. Fluid Mech.* 220:397–411, 1990.

[19] Saad, Y. and M. H. Schultz. GMRES: a generalized minimal residuals algorithm for solving nonsymmetric linear systems. *Math. Comput.* 44:417–424, 1983.

[20] Schoephoerster, R. T., F. Oynes, G. Nunez, M. Kapadvanjwala, and M. K. Dewanjee. Effects of local geometry and fluid dynamics on regional platelet deposition on artificial surfaces. *Arterioscler. Thromb.* 13:1806–1813, 1993.

[21] Stein, P. D. and H. N. Sabbah. Measured turbulence and its effect on thrombus formation. *Circ. Res.* 35:608–614, 1974.

[22] Thornburg, H. J., U. Ghia, G. A. Osswald, and K. N. Ghia. Efficient computation of vortical flow using flow-adaptive time-dependent grids. *Fluid Dyn. Res.* 10:371–397, 1992.

[23] White, F. M. Fluid Mechanics. New York: McGraw-Hill, 1979, pp. 278–279.

[24] Wilcox, D. C. Turbulence Modeling for CFD. La Canada, California: DWC Industries, 1993.

[25] Wilcox, D. C.. Simulation of transition with a two-equation turbulence model. *AIAA J.* 32:247–255, 1994.

[26] Willert, C. E. and M. Gharib. Digital particle image velocimetry. *Exp. Fluids* 10:181–193, 1991.

[27] Wurzinger, L. J. and H. Schmid-Schoenbein. The role of fluid dynamics in triggering and amplifying hemostatic reactions in thrombogenesis. Blood flow in large arteries: Application to Atherogenesis and Clinical Medicine. Monogr. Atheroscler. Liepsch (ed): Basel, Karger, 1990, Vol. 15, pp. 215–226.

[28] Yellin, E. L.. Laminar-turbulent transition process in pulsatile flow. *Circ. Res.* 19:791–804, 1966.

[29] Yoganathan, A. P., N. H. Corcoran, E. C. Harrison, and J. R. Carl. The Bjork-Shiley aortic prosthesis: Flow characteristics, thrombus formation and tissue overgrowth. *Circulation* 53:70–75, 1978.

[30] Young, D. F.. Fluid mechanics of arterial stenosis. *J. Biomech. Eng.* 101:157–175, 1979.